Clays and Clay Minerals, Vol. 44, No. 6, 791–800, 1996.

CHARACTERIZATION OF SOIL CLAY MINERALS: DECOMPOSITION OF X-RAY DIFFRACTION DIAGRAMS AND HIGH-RESOLUTION ELECTRON MICROSCOPY

DOMINIQUE RIGHI[1] AND FRANÇOISE ELSASS[2]

[1] URA 721 CNRS "Argiles, Sols et Altérations", Faculté des Sciences, 86022 Poitiers Cedex, France

[2] Station de Science du Sol, INRA, 78026 Versailles Cedex, France

Abstract—Fine clays (<0.1 μm) extracted from an acid soil developed in a granite saprolite from the Massif Central, France, were characterized by X-ray diffraction (XRD) using a curve decomposition program, and high-resolution transmission electron microscopy (HRTEM) associated with a method of impregnation of moist samples. Direct measurement of *d*-spacings were performed on HRTEM photographs. Decomposition of XRD patterns indicated 5 to 6 different clay phases including chlorite (and/or hydroxy-interlayered vermiculite), vermiculite/smectite, illite/vermiculite and illite/smectite mixed layers. Expandable phases with decreasing layer charge (vermiculite, high- and low-charge smectite) were shown in the clay assemblage. When performed on K-saturated samples subjected to wetting and drying cycles, HRTEM observations were consistent with the XRD results. The major clay mineral phases identified by the decomposition of XRD patterns were also found by direct measurement of *d*-spacings on HRTEM images. Vermiculite and high-charge smectite appeared to be impregnated with preservation of their initial hydration state, whereas low-charge smectite interlayers were penetrated by the resin molecules during the impregnation procedure. It was concluded that the decomposition of XRD patterns gave a realistic analysis of the clay phases present in a complex soil clay sample, as well as the direct measurement of a limited number (50) of clay crystals on HRTEM images.

Key Words—Acid Soil, Decomposition of X-ray Patterns, High-Charge Smectite, High-Resolution Electron Microscopy, Illite/Smectite Mixed Layers, Illite/Vermiculite Mixed Layers, Low-Charge Smectite, Soil Clays, X-ray Diffraction.

INTRODUCTION

Because in temperate soils the clay fractions are complex mixtures of numerous clay mineral phases, including mixed-layer minerals of different types, their characterization is generally a difficult task. These mixtures exhibit complex XRD bands combining several poorly individualized maxima. As a result, comparison of experimental diffraction peak positions with reference tables does not permit precise identification of the constituting clay minerals. Analysis of XRD patterns using a curve decomposition program (Lanson 1993) greatly improves identification of the different clay phases. However, decomposition is no more than a mathematical treatment of the XRD diagram, and elementary curves which have no mineralogical signification may be computed in fitting with the experimental diagram. Validation of the decomposition procedure was made (Lanson and Besson 1992; Lanson and Velde 1992), but essentially for diagenetic series with illite/smectite mixed-layer clays, a simpler case than a soil clay assemblage. To date, no attempt has been made to validate the results obtained by decomposition of XRD patterns when performed on soil clay fractions.

HRTEM was also used to characterize soil clay minerals (Elsass and Robert 1992; Romero et al. 1992; Aoudjit et al. 1995). Representativity of HRTEM observations is questionable according to the very small number of clay particles that can be observed, as compared with the millions of those "seen" by XRD. Another problem with HRTEM is the dehydration of the clay during sample preparation and subsequent collapse of vermiculite and smectite layers to *d*-spacings of 1.00 nm. This results in ambiguity in differentiation between illite-, vermiculite- and/or smectite-like lattice fringes. Tessier (1984) developed a method of impregnation of moist samples that maintains layer staking sequences and causes smectites to be permanently expanded for HRTEM observations. The method was recently tested by Kim et al. (1995), and appeared to allow unambiguous identification of illite and smectite interlayers in lattice fringe images.

The purpose of this study was to compare the information obtained on fine clay fractions (<0.1 μm) extracted from an acid soil developed from a granite saprolite, using either decomposed XRD patterns or HRTEM.

SOIL MATERIAL

Clays were separated from an Ochric Podzosol (Référentiel Pédologique, INRA 1992) or Entic Haplorthod (Soil Taxonomy) developed from a granite saprolite of the Plateau de Millevaches, Massif Central, France. The soil, located on a summit position at an elevation of 925 m, was selected as a good example of those widely distributed in this region. Some char-

Table 1. Some characteristics of the soil horizons.

Horizon	A1	Bh	Bw	C
Depth cm	0–15	15–35	35–50	>50
pH (H_2O)	4.8	5.1	5.1	5.1
Clay (<2 μm) g kg^{-1}	116	96	79	73
Organic carbon g kg^{-1}	77	43	22	11
Fe_2O_3 CBD g kg^{-1}	13.3	12.0	8.4	6.8
Al_2O_3 CBD g kg^{-1}	13.7	18.2	14.7	9.1
CEC $cmol_c$ kg^{-1}	24.4	15.7	16.5	7.1

acteristics of the soil horizons are listed in Table 1. A short description of the profile is given below.

0–15 cm: Al, very dark brown (10YR 2/2) sandy loam, organic rich, strong fluffy structure, friable, many roots, clear wavy boundary.

15–35 cm: Bh, dark brown (10YR 3/3) sandy loam, weak, subangular blocky structure, friable, few roots, clear wavy boundary.

35–50 cm: Bw, dark yellowish brown (10YR 3/4) sandy loam, weak subangular blocky structure, granite gravels, few roots, diffuse smooth boundary.

>50 cm: C, dark yellowish brown (10YR 4/4) gravelly material.

METHODS

The clay fractions (<2 μm) were obtained from the soil samples by sedimentation after destruction of organic matter with diluted, Na-acetate-buffered H_2O_2 and dispersion at pH = 9 (NaOH). After treatment with citrate-bicarbonate-dithionite to remove iron oxides and oxyhydroxides, the bulk clay fraction was divided into fine (<0.1 μm) and coarse (0.1–2 μm) clay subfractions using a Beckman J2-21 centrifuge equipped with the JCF-Z continuous flow rotor.

X-ray Diffraction

XRD diagrams were obtained from oriented specimens using a Philips diffractometer with Fe-filtered Co*K*α radiation. The diffractograms were recorded numerically by a DACO-MP recorder associated with a microcomputer using the Diffrac AT software (SOCABIM, France). The XRD diagrams were then decomposed into their elementary component curves using the DECOMPXR program of Lanson (1993). By running a large series of tests, Lanson (1990) demonstrated that the standard deviation on curve characteristics determination is induced mostly by the experimental equipment and that the calculated characteristics are representative of the sample studied. Lanson and Besson (1992) indicated also that a minimum difference of 0.3 °2θ on peak position and 0.2 °2θ on width is necessary for DECOMPXR to separate the contributions of 2 phases. The difference required for one parameter may be smaller if the difference for the other is larger, even though the elementary curve parameters (width, position, intensity) are computed independently. Background intensities were subtracted, assuming they were distributed as a straight-line curve joining the limits of the portion of the experimental diagram subjected to decomposition. The XRD patterns were decomposed by progressively increasing the number of elementary curves, in order to obtain a good fit with the smallest number of curves.

Pretreatments of the specimens included Ca-saturation and solvation with ethylene glycol and K-saturation and heating at 350 °C. High-charge to low-charge smectites layers were identified on the basis of re-expansion with glycerol of K-saturated samples (Malla and Douglas 1987) subjected to wetting and drying cycles. Wetting and drying cycles (W/D) in the presence of K ions were conducted by mixing 100 mL of 1 *M* KCl solution with 100 mg of fine clay in glass beakers, and then by drying them at 60 °C. After drying, distilled water was added, and the drying cycle repeated. Sixty cycles were performed. After reaction, samples were thoroughly washed until chloride-free.

Chemical Analysis

Bulk chemical analyses were performed on the <0.1-μm subfractions according to the procedure described by Jeanroy (1972). Si, Al, Fe, Ti, Mg, Ca, Na and K were analyzed by atomic absorption spectroscopy (AAS). Loss on ignition at 1100 °C was measured by thermogravimetric analysis (TGA) (Netzsch STA 409 EP). Accessible structural charge was measured using the Cs-adsorption method developed by Anderson and Sposito (1991).

Microscopy and Image Interpretation

The K-saturated samples subjected to W/D cycles were used for HRTEM observations. The samples were processed using the technique of Tessier (1984). Randomly oriented pastes of fine clay fractions coated with agar were equilibrated at 32 hPa with pure water for 24 to 48 h. After rehydration, water was removed with methanol, and the methanol was removed with LR White resin, a polymer of low viscosity. After polymerization of the resin at 60 °C, the samples were sectioned at 50 nm by ultramicrotomy using a Reichert Ultracut E microtome.

One-dimensional HRTEM and bright-field lattice fringe imaging was performed on numerous fields for each sample. The microscope was a Philips 420 STEM working at 120-kV accelerating voltage with a 40-μm objective aperture, eliminating lattice periodicities smaller than 0.35 nm. Photographs were taken in underfocus conditions, the optimal defocus being determined between 100 and 150 nm in order to visualize simultaneously both 1.0- and 1.4-nm periodicities with a favorable transfer efficiency in the microscope. Zero focus is obtained on the carbon support. The preset magnification of × 51,000 was applied (accuracy of magnification is regularly checked with a standard

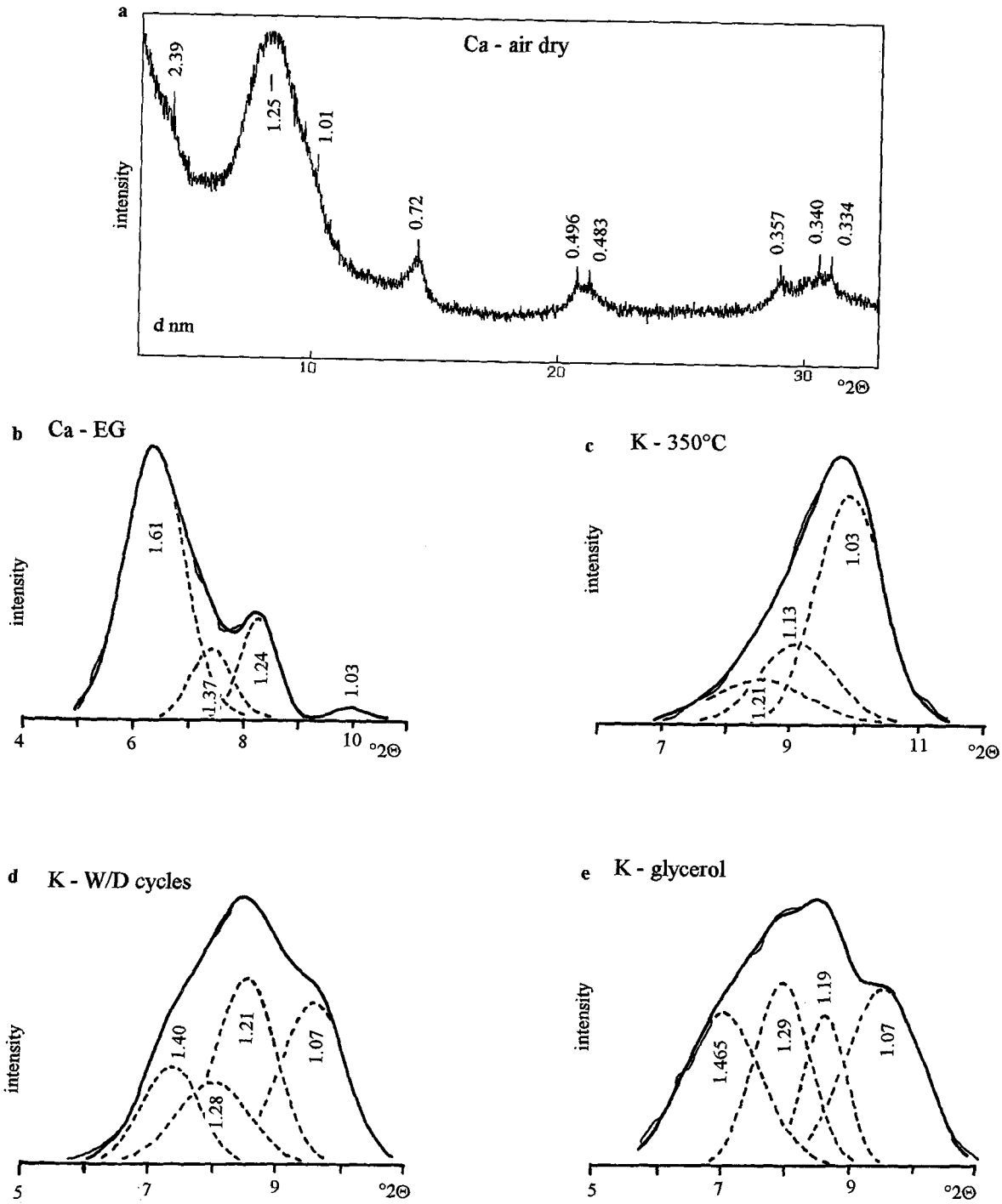

Figure 1. XRD patterns for the A1 sample. a) experimental diagram, Ca-saturated, air-dried sample; b) Ca-saturated, ethylene-glycol-solvated sample; c) K-saturated sample heated to 350 °C; d) K-saturated sample subjected to wetting and drying cycles, room temperature; e) K-saturated sample subjected to wetting and drying cycles, glycerol-solvated. Co$K\alpha$ radiation —— experimental curve; – – – elementary computed curve; ▬▬ best fit computed curve.

https://doi.org/10.1346/CCMN.1996.0440610 Published online by Cambridge University Press

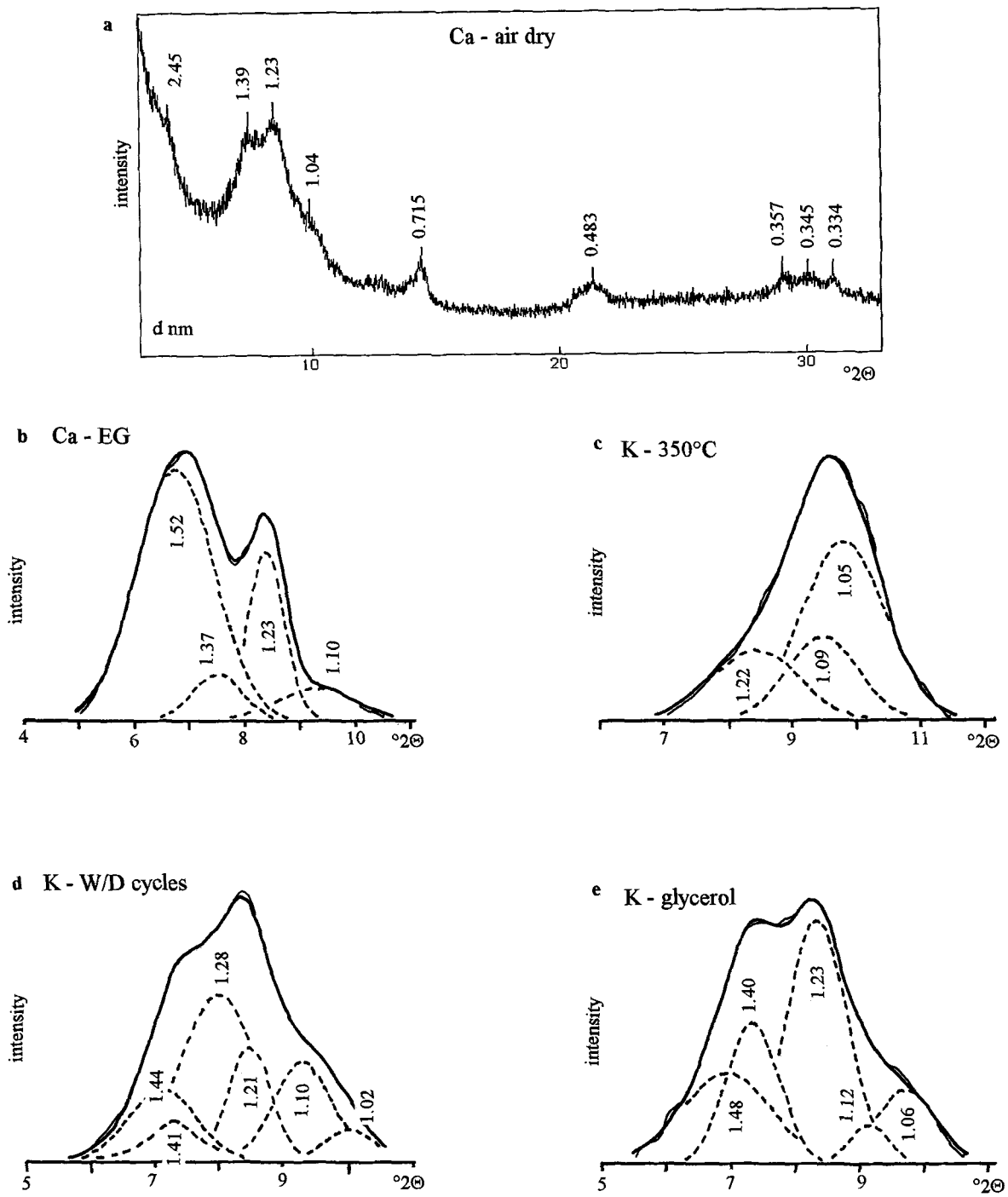

Figure 2. XRD patterns for the Bh sample. a) experimental diagram, Ca-saturated, air-dried sample; b) Ca-saturated, ethylene-glycol-solvated sample; c) K-saturated sample heated to 350 °C; d) K-saturated sample subjected to wetting and drying cycles, room temperature; e) K-saturated sample subjected to wetting and drying cycles, glycerol-solvated. Co$K\alpha$ radiation —— experimental curve; – – – elementary computed curve; ▬▬ best fit computed curve.

https://doi.org/10.1346/CCMN.1996.0440610 Published online by Cambridge University Press

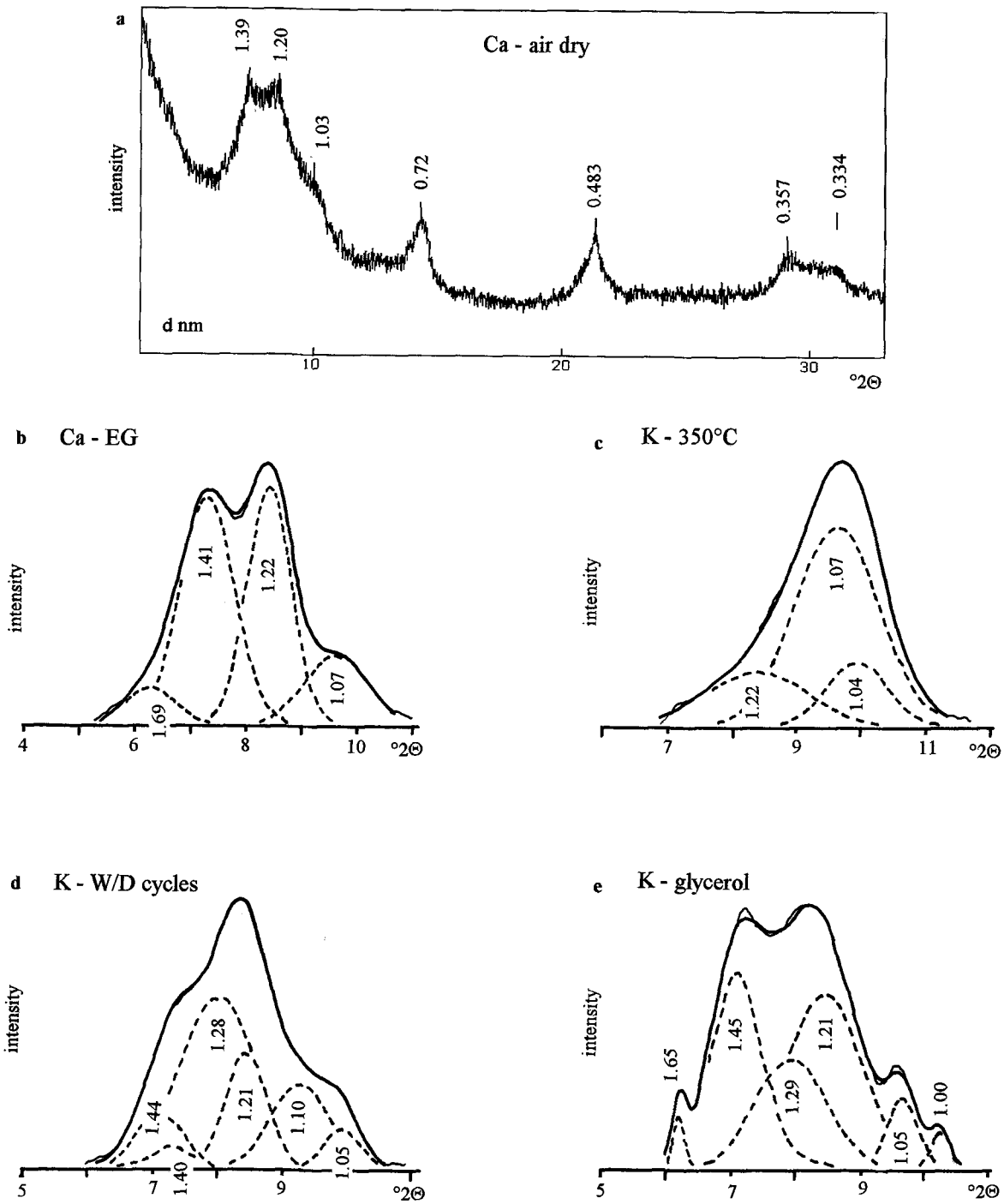

Figure 3. XRD patterns for the Bw sample. a) experimental diagram, Ca-saturated, air-dried sample; b) Ca-saturated, ethylene-glycol-solvated sample; c) K-saturated sample heated to 350 °C; d) K-saturated sample subjected to wetting and drying cycles, room temperature; e) K-saturated sample subjected to wetting and drying cycles, glycerol-solvated. Co$K\alpha$ radiation —— experimental curve; – – – elementary computed curve; ▬▬ best fit computed curve.

https://doi.org/10.1346/CCMN.1996.0440610 Published online by Cambridge University Press

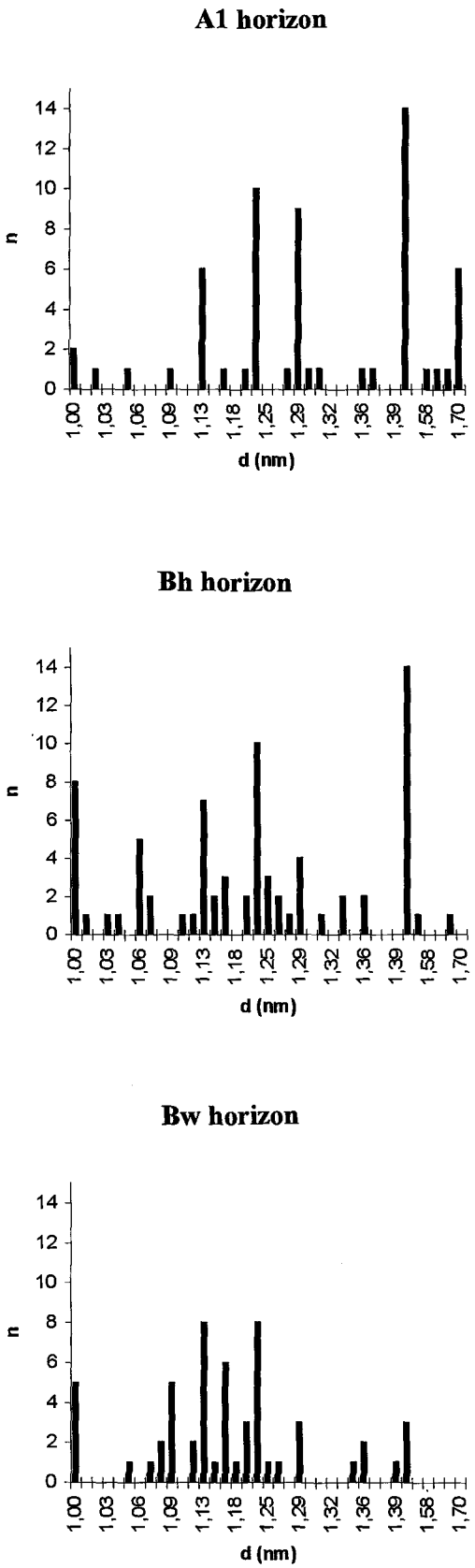

mica sample). Measurements of the images were made directly from the negatives by means of a stereo-microscope equiped with a micrometric scale. Error on one measurement was estimated to 0.02 nm.

Values of interlayer spacings were obtained by dividing the thickness of the stack of layers by the number of interlayers. Thickness was measured between the centers of the 2 external layers, at the maximum intensity of the lattice fringe. Only stacks of layers of strictly parallel orientation (called "crystals" according to the nomenclature of Tessier 1984, and regarded as the coherent scattering domains from the viewpoint of XRD), either present as individual small particles or as sub-units of larger quasi-crystals, were measured. At least 50 crystals were measured for each sample.

RESULTS

XR Diffraction

Al HORIZON SAMPLE. The decomposition of the XRD diagram for the glycolated sample in the 4–11 °2θ region gave 4 basic curves with maximum intensities at d = 1.610, 1.384, 1.240 and 1.033 nm (Figure 1b). In the 18–23 °2θ region, 5 peaks were obtained at d = 0.542, 0.520, 0.496, 0.483 and 0.471 nm (not shown) and 5 peaks were observed at d = 0.357, 0.350, 0.340, 0.334 and 0.326 nm in the 28–33 °2θ region (not shown).

According to simulations with the NEWMOD program (Reynolds 1985), the peak at 1.610 nm associated with that at 0.340 nm was attributed to vermiculite (or chlorite)/smectite mixed layers with approximately 80% smectite. Associated with those at d = 0.483 and 0.350 nm, the peak at 1.384 nm indicated illite/vermiculite (or chlorite) mixed layers with 80% vermiculite. The peak at 0.124 nm associated with the superstructure reflection near 2.450 nm was taken as evidence for a fully ordered interstratified illite/vermiculite (or chlorite) mineral with 50% illite. The peaks at d = 1.033, 0.496 and 0.334 nm indicated illitic layers and those at d = 0.542 and 0.521 nm in the 18–23 °2θ region were typical of illite/smectite mixed layers with either 50 or 80% illite. The peak at 0.471 nm in the 18–23 °2θ region indicated chlorite layers, and that at 0.357 in the 28–33 °2θ region indicated kaolinite layers.

Three basic curves with their maximum at 1.207, 1.129 and 1.035 nm were obtained from the XRD diagram of the sample K-saturated and heated to 350 °C (Figure 1c) indicating interstratification with uncollapsed layers with a hydroxide sheet (chlorite and/or hydroxy-Al vermiculite layers). The lack of peak near

←

Figure 4. Histograms of HRTEM measurements. n: number of measured crystals with a given d-spacings; d(nm): average d-spacing in measured crystals (d = total thickness of the crystal divided by the number of interlayers).

https://doi.org/10.1346/CCMN.1996.0440610 Published online by Cambridge University Press

Table 2. Data obtained from measurements of HRTEM images.

		A1 horizon				
†	d (nm)	1.13	1.21	1.29	1.45	1.70
‡	n crystals	6	10	9	14	6
§	N_{min}; N_{max}	4; 7	2; 9	4; 7	2; 8	3; 5
	N (average)	5	4	4	4	3
		Bh horizon				
	d (nm)	1.00	1.06	1.13	1.21	1.45
	n crystals	8	5	7	10	13
	N_{min}; N_{max}	4; 11	5; 5	4; 10	3; 5	2; 7
	N (average)	8	5	5	4	4
		Bw horizon				
	d (nm)	1.00	1.09	1.13	1.16	1.21
	n crystals	5	5	7	6	8
	N_{min}; N_{max}	3; 13	5; 5	4; 13	6; 11	3; 9
	N (average)	7	5	7	7	5

† d(nm): average d-spacings in measured crystals (d = total thickness of the crystal divided by the number of interlayers).
‡ n: number of measured crystals with a given d-spacing.
§ N_{min}; N_{max}: minimum and maximum number of layers in measured crystals.

1.40 nm was attributed to a low thermal stability of the chlorite, as often observed for weathered chlorite (Righi et al. 1993).

The XRD diagram from the K-saturated sample subjected to W/D cycles was decomposed in the 5–11 °2θ region. Four basic curves were obtained with their maxima at d = 1.400, 1.284, 1.210 and 1.075 nm (Figure 1d). The peak at 1.400 nm indicated uncollapsed layers of chlorite and/or hydroxy-interlayered vermiculite. The peak at 1.210 nm was taken as evidence for single-layer water smectite, but part of its intensity could be given by interstratification of uncollapsed layers (1.400 nm) with illitic layers. The 1.075-nm peak was attributed to interstratification of illitic layers and/or fully collapsed vermiculite with smectite or vermiculite layers in the single-layer water hydratation state (d = 1.210 to 1.160 nm). The peak at d = 1.284 nm was interpreted as single-layer water smectite/uncollapsed (1.40-nm) mixed layers. Simulation of this peak position with NEWMOD required a proportion of 20% of uncollapsed layers (chlorite or hydroxy-vermiculite), that was consistent with the peak at d = 1.610 nm observed in the glycolated sample.

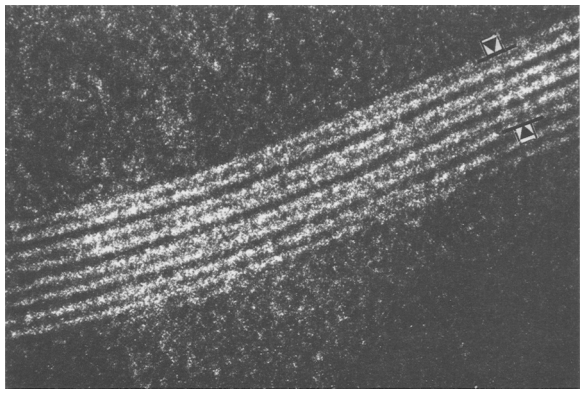

Figure 6. Mixed-layer mineral: average d-spacing = 1.06 nm, obtained with 3 interlayers at 1.00 nm and 2 at 1.16 nm.

Following glycerol solvation, the same 4 basic curves were found, but the relative intensity of the peak near d = 1.29 nm (Figure 1e) was increased and the peak at d = 1.40 nm was shifted to 1.465 nm. That was taken as evidence of the formation of 2-layer glycerol complexes with low-charge smectite layers.

Bh HORIZON SAMPLE. The decomposition of the XRD diagram for the Ca-saturated and glycol-solvated sample gave 4 basic curves with their maximum intensities at d = 1.524, 1.374, 1.226 and 1.103 nm (Figure 2b). As for the Al horizon sample, the peak at 1.524 nm was attributed to vermiculite (or chlorite)/smectite mixed layers, but with a lower proportion of smectite (30% according to NEWMOD simulation). The 2 peaks at 1.374 and 1.226 nm led to the same attribution as the peaks at 1.384 and 1.240 nm in the Al horizon sample. The peak at 1.103 nm indicated illite/vermiculite (or chlorite) mixed layers with approximately

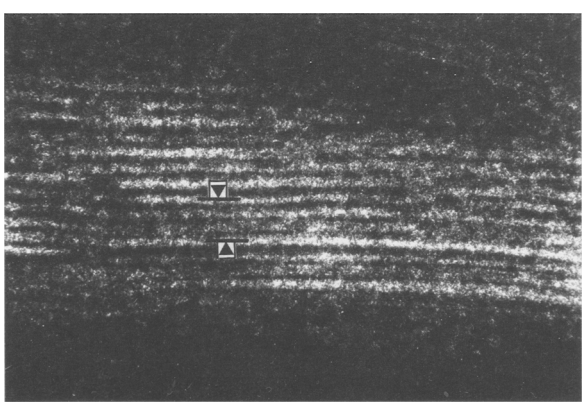

Figure 5. Illitic layers (average d-spacing = 1.00 nm).

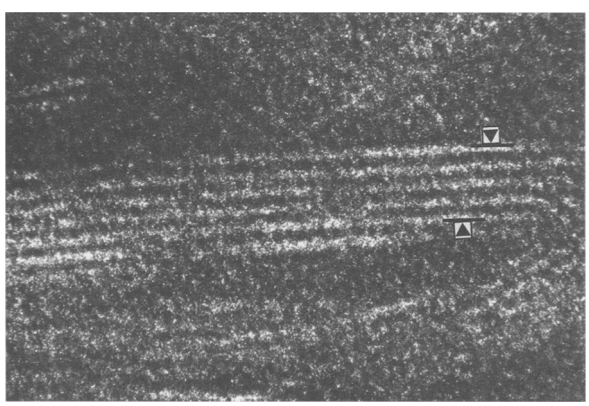

Figure 7. Stack of interlayers with d-spacing = 1.21 nm.

https://doi.org/10.1346/CCMN.1996.0440610 Published online by Cambridge University Press

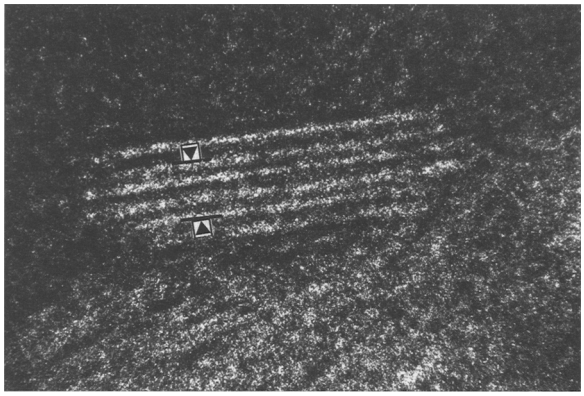

Figure 8. Mixed-layer mineral: average d-spacing = 1.29 nm, obtained with 2 interlayers at 1.36 nm and one at 1.18 nm.

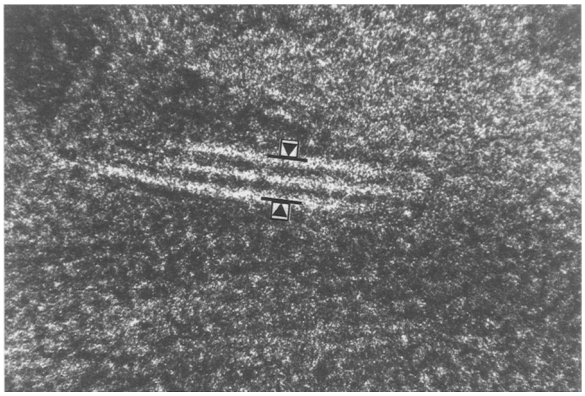

Figure 9. Individual crystal with 1.44 nm d-spacing (chlorite remnant?).

80% illite. In the 18–23 °2θ region (not shown), no peak characteristic of illite/smectite mixed layers was observed in this sample.

The XRD diagram from the K-saturated and heated sample was identical to that of the equivalent sample from the Al horizon (Figure 2c).

The decomposition of XRD diagram from the K-saturated sample subjected to W/D cycles gave quite the same basic curves (Figure 2d) as the equivalent A1 horizon sample, except that 2 basic curves were found with their maximum near 1.40 nm, indicating 2 different mineral phases that could be chlorite (1.408 nm) and hydroxy-vermiculite (1.440 nm). In this sample, the 1.281 nm peak was the most intense, but not the one at 1.210 nm, as with the A1 sample. That could be attributed to a greater amount of uncollapsed (1.40-nm) layers in the Bh sample. Following glycerol solvation, a curve with its maximum at $d > 1.40$ nm, indicating low-charge smectite layers (2-layer glycerol complexes), was also observed in this sample (Figure 2e). The peak at 1.281 nm present in the K-saturated W/D sample was absent after glycerol solvatation, but a peak at 1.399 nm was observed. That could be interpreted by the transformation in the 1.281-nm mixed-layer phase of the single-layer water smectite component by a single-layer glycerol smectite complex (d = 1.39 nm); therefore, this smectite would be of a high-charge type.

Bw HORIZON SAMPLE. The decomposition of XRD diagram from the Ca-saturated, glycol-solvated sample gave 4 basic curves with their maxima at d = 1.634, 1.407, 1.221 and 1.066 nm (Figure 3b). The intensity of the 1.634 peak was very low, with the 2 most intense peaks at d = 1.047 and 1.221 nm. Compared to the Bh sample, the relative intensity of the peak between 1.00 and 1.10 nm (illite-rich phase) was greater in this sample. Attribution of the peak at 1.407 and 1.221 nm was the same as for the equivalent peaks in the A1 and Bh samples.

Three basic curves were obtained by decomposition of the XRD diagram from the K-saturated and heated sample (Figure 3c). Compared to the 2 other equivalent samples, the position of the most intense peak (1.067 nm) was shifted toward small 2θ angles, indicating a larger proportion of uncollapsed layers (chlorite and/or hydroxy-Al vermiculite) in this sample.

The decomposition of the XRD diagram from the K-saturated W/D sample (Figure 3d) gave the same basic curves as for the equivalent Bh sample. Peak positions were not affected by glycerol solvation. Only the relative intensities of the peaks near 1.28 and 1.44 nm were changed; the first one decreased, while the second increased (Figure 3e). As for the Bh sample, this suggested the occurrence of high-charge smectite layers.

HRTEM Observations

The number of interlayers measured in one crystal varied from 1 (bi-layer crystal) to a maximum of 15. The average number ranged from 4 (A1 horizon sample) to 6 (Bw horizon). The lateral extent of the crystals was rather short, the average size being 30–40 nm.

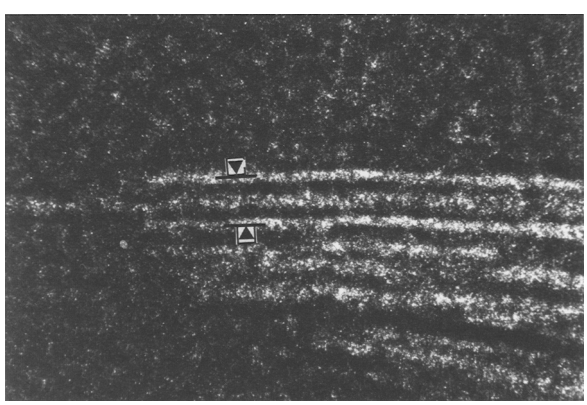

Figure 10. Two interlayers with 1.70 nm d-spacing.

https://doi.org/10.1346/CCMN.1996.0440610 Published online by Cambridge University Press

Table 3. Total analyses (% 105 °C dry sample) and accessible permanent charge ($cmol_c\ kg^{-1}$) of the fine clay (<0.1-μm) fractions.

	SiO_2	Al_2O_3	Fe_2O_3	MnO	MgO	CaO	Na_2O	K_2O	TiO_2	LOI†	Ac Per Ch‡
A1	43.42	22.22	9.85	0.07	2.31	0.54	0.62	1.61	2.02	17.25	37.4
Bh	41.08	24.72	9.42	0.08	2.52	0.22	0.41	1.64	1.71	17.76	33.3
Bw	42.34	19.01	7.72	0.05	2.81	0.25	0.43	1.76	1.48	24.31	28.9

† LOI: loss on ignition.
‡ Ac Per Ch: accessible permanent charge.

Histograms of the measured *d*-spacing values obtained from the 3 samples are given in Figure 4. In one sample, almost all of the measured *d*-spacings were distributed between 5 values only (Table 2), which changed according to the sample. Crystals with *d*-spacings of 1.70 and 1.29 nm were abundant in the A1 horizon sample only. Spacings at 1.45 nm were found in the 3 samples, but with lesser amounts in the Bw horizon sample. Crystals with *d*-spacings at 1.00, 1.06 or 1.09 nm were abundant in the Bh and Bw horizon samples, but not in the A1 sample. A clear general tendency was larger *d*-spacings in the A1 horizon sample than in the 2 others. Crystals with *d*-spacings at 1.00 nm were typically illitic material (Figure 5), while those with larger *d*-spacings (1.06, 1.09 and 1.13 nm) appeared as ordered interstratification of 2 types of interlayer, probably illite and collapsed vermiculite (Figure 6). Crystals with 1.21, 1.29, 1.45 and 1.70 nm *d*-spacings (Figures 7, 8, 9 and 10) did not exhibit any specific feature: however, different types of interlayer were observed in crystals with *d*-spacings at 1.29 nm, indicating random interstratification (Figure 8).

Chemical Analysis and Accessible Permanent Charge

Total chemical analyses of the 3 samples are given in Table 3. In good agreement with XRD, MgO and K_2O content decreased from the Bw to the A1 sample, indicating a decrease in the amount of chloritic and illitic layers, respectively. The increase of the accessible permanent charge (28.9 to 37.4 $cmol_c\ kg^{-1}$) from the Bw to the A1 sample (Table 3) was also in good agreement with higher amounts of smectite layers in the A1 sample.

DISCUSSION

As indicated by the decomposition of the XRD diagrams, the clay assemblage in the 3 samples was constituted with 5 to 6 mineral phases including chlorite (and/or hydroxy-interlayered vermiculite), vermiculite(chlorite)/smectite, illite/vermiculite and illite/smectite mixed layers. Expandable phases (vermiculite, high- and low-charge smectite) with decreasing layer charge were shown in this assemblage. The identified clay mineral phases were those expected to be found in a temperate acid soil developed on granite saprolite. The general evolution of clays observed in this soil (weathering of chlorite, removal of interlayered hydroxide sheet and formation of illite/smectite mixed layers and smectite) was not different from that already described for similar soils (Righi and Meunier 1991; Righi et al. 1993), but the genetic interpretation of these clay assemblages was beyond the scope of this study.

The *d*-spacing values measured on HRTEM pictures from these soil clay samples were more diversified than those described for diagenetic clays. Środoń et al. (1990) found only 2 *d*-spacing values at 1.35 and 1.00 nm attributed to smectite and illite layers, respectively. Kim et al. (1995) measured *d*-spacings at 1.20 and 1.30 nm, both attributed to smectite layers. In samples from acid soils, Elsass and Robert (1992) attributed spacings as high as 1.40 nm to hydroxy-Al vermiculite, but those at 1.35 nm to smectite layers with a single-layer methacrylate molecule (thickness 0.35 nm) interlayered.

Interactions between clay layers, water, methanol and the resin used during the impregnation procedure are not yet fully understood. Kim et al. (1995) suggested that smectite layers were only partially dehydrated by methanol and that water molecules remained in the interlayer and caused a limited layer expansion, depending on the layer charge as well as the nature of the interlayer cation. Their polar character allows the components of the LR White resin to adsorb on clay surfaces. The configuration of the molecules depends on the selectivity of clay surfaces, which can differ from one sample to another. We speculated that the different *d*-spacings observed might be due to differences in the ability of LR White resin components to cause expansion of clay minerals with variable layer charge. According to the hypothesis of Elsass and Robert (1992), interlayers with *d*-spacing values greater than 1.00 but smaller than 1.35 nm should be free of resin. Therefore, we postulated that they were embedded with preservation of interlayered water molecules.

HRTEM observations were consistent with the results given by the decomposition of XRD diagrams from K-saturated samples subjected to W/D cycles. That treatment caused the partial dehydration of the smectite layers (formation of single-layer water complexes) and the complete and irreversible collapse of vermiculite layers. For the A1 horizon sample, 4 basic

curves with their maxima at 1.40, 1.28, 1.21 and 1.075 nm were obtained by decomposition of the XRD diagram. These peaks could be attributed to the crystals with *d*-spacings measured at 1.45, 1.29, 1.21 and 1.13 nm on HRTEM pictures. According to HRTEM observations, crystals with *d*-spacings at 1.70 nm were a major component of the clay assemblage. They could be attributed to smectite layers with molecules of resin interlayered. In this sample, solvation with glycerol has shown that a 2-layer glycerol complex was formed with the low-charge K-saturated smectite layers. Although the organic molecule was not the same, that supported the hypothesis of possible penetration of resin components in the interlayer of low-charge smectite saturated with monovalent cation.

Identical remarks could be made for the Bh and Bw horizon samples. Moreover, the lower proportion of smectite layers, which were mainly high-charge layers (XRD result) in these 2 samples, was in good agreement with the lack of crystals with *d*-spacings at 1.70 nm on their HRTEM pictures. The greater amount of crystals with *d*-spacings at 1.00 nm in the Bh and Bw samples was also consistent with the XRD peaks near 1.03 nm found by decomposition in these samples, but not in the A1 horizon. Both techniques, HRTEM and decomposition of XRD diagrams, indicated more illitic layers and less smectite (especially low-charge) layers in the Bh and Bw horizon samples than in the A1 one.

CONCLUSION

Characterization of clay minerals in the fine clay (<0.1-μm) fraction of a temperate acid soil, either by HRTEM or decomposition of XRD diagrams, gave consistent results. Expandable layers (vermiculite, high- and low-charge smectite) behave differently when subjected to the Tessier's impregnation procedure needed for HRTEM observations. In K-saturated samples, the resin molecules would penetrate low-charge smectite interlayers only, but vermiculite and high-charge smectite layers appeared to have been embedded in the resin with preservation of their initial hydration state. This behavior was more or less similar to that of K-saturated samples solvated with glycerol.

Peak positions for the basic curves obtained by decomposition of the XRD diagrams indicated *d*-spacings in good agreement with those measured directly on crystals by HRTEM. Therefore, it appeared that decomposition of XRD diagrams gave a realistic analysis of complex clay assemblages. From the other side, HRTEM observations with the measurement of a limited number of crystals (about 50) also led to a valuable estimation of the different components in the clay mixture. Moreover, the chemical composition of the main components might be obtained using analytical electron microscopy.

REFERENCES

Anderson SJ, Sposito G. 1991. Cesium-adsorption method for measuring accessible structural surface charge. Soil Sci Soc Am J 55:1569–1576.

Aoudjit H, Robert M, Elsass F, Curmi P. 1995. Detailed study of smectite genesis in granite saprolites by analytical electron microscopy. Clay Miner 30:135–148.

Elsass F, Robert M. 1992. Application of high resolution electron microscopy to soil clay origin and organization in a temperate climate. Geologica Carpathica Ser Clays 2:55–61.

INRA 1992. Référentiel Pédologique. Principaux sols d'Europe. Paris: Institut National de la Recherche Agronomique (INRA). 222 p.

Jeanroy E. 1972. Analyse totale des silicates naturels par spectrophotometrie d'absorption atomique. Application au sol et à ses constituants. Chim Anal 54:159–166.

Kim J-W, Peacor DR, Tessier D, Elsass F. 1995. A technique for maintaining texture and permanent expansion of smectite interlayers for TEM observations. Clays Clay Miner 43:51–57.

Lanson B. 1990. Mise en évidence des mécanismes de transformation des interstratifiés illite/smectite au cours de la diagenése [thesis]. Paris: Univ of Paris VI. 366 p.

Lanson B. 1993. DECOMPXR, X-ray diffraction pattern decomposition program. Poitiers, France: ERM. 48 p.

Lanson B, Besson G. 1992. Characterization of the end of smectite-to-illite transformation: decomposition of the X-ray patterns. Clays Clay Miner 40:40–52.

Lanson B, Velde B. 1992. Decomposition of X-ray diffraction patterns: a convenient way to describe complex I/S diagenetic evolution. Clays Clay Miner 40:629–643.

Malla PB, Douglas LA. 1987. Identification of expanding layer silicates: layer charge vs. expansion properties. In: Schultz LG, van Olphen H, Mumpton FA, editors. Proceedings of the International Clay Conference; 1985; Denver. Bloomington, Indiana: The Clay Minerals Society. p 227–283.

Reynolds RC. 1985. Description of program NEWMOD for the calculation of the one-dimensional X-ray diffraction patterns of mixed-layered Clays. Hanover, New Hampshire: Reynolds RC, 8 Brook Road. 24 p.

Righi D, Meunier A. 1991. Characterization and genetic interpretation of clays in an acid brown soil (Dystrochrept) developed in a granitic saprolite. Clays Clay Miner 39: 519–530.

Righi D, Petit S, Bouchet A. 1993. Characterization of hydroxy-interlayered vermiculite and illite/smectite interstratified minerals from the weathering of chlorite in a Cryorthod. Clays Clay Miner 41:484–495.

Romero R, Robert M, Elsass F, Garcia C. 1992. Abundance of halloysite in soils developed from crystalline rocks. Contribution of transmission microscopy. Clay Miner 39:137–141.

Środoń J, Andreoli C, Elsass F, Robert M. 1990. Direct high-resolution transmission electron microscopic measurement of expandability of mixed-layer illite/smectite in bentonite rock. Clays Clay Miner 38:373–379.

Tessier D. 1984. Etude expérimentale de l'organisation des matériaux argileux [thesis]. Paris: Univ of Paris VII. Versailles, France: INRA. 361 p.

(Received 26 October 1995; accepted 15 February 1996; Ms. 2703)